

Topological states in the noncentrosymmetric superconductors LaPtSi and LaPtGeXianbiao Shi^{1,2}, Qingbo Liu,³ Peng He,^{1,2,*} Yunhuan Yuan,^{1,2,4} Xiangpeng Kong,² Kang Li,^{2,†} and Weiwei Zhao^{1,2,4,‡}¹State Key Laboratory of Advanced Welding & Joining, Harbin Institute of Technology, Harbin 150001, People's Republic of China²Flexible Printed Electronics Technology Center, Harbin Institute of Technology (Shenzhen), Shenzhen 518055, People's Republic of China³School of Physics and Wuhan National High Magnetic Field Center, Huazhong University of Science and Technology, Wuhan 430074, People's Republic of China⁴Key Laboratory of Micro-systems and Micro-structures Manufacturing of Ministry of Education, Harbin Institute of Technology, Harbin 150001, People's Republic of China

(Received 21 October 2021; accepted 8 December 2021; published 16 December 2021)

The interaction between bulk Dirac points and *s*-wave bulk superconductivity can sustain an exotic quasi-particle excitation, namely, a gapless one-dimensional helical Majorana mode. Herein, based on first-principles calculations, we predict that noncentrosymmetric superconductors LaPtSi and LaPtGe are Dirac superconducting semimetal candidates. Without spin-orbit coupling (SOC), LaPtSi and LaPtGe show three-dimensional metallic behavior with a normal band order. SOC induces energy level splitting and reordering, resulting in two pairs of bulk Dirac points with type-II and type-III characteristics and a topological insulator state in the Γ -Z direction. The obtained nonzero topological \mathbb{Z}_2 invariants and multiple nontrivial surface states on the (001) surface directly demonstrate the nontrivial topological features of LaPtSi and LaPtGe. Thus, these predicted compounds provide realistic platforms for the interplay of bulk Dirac points and superconductivity.

DOI: [10.1103/PhysRevB.104.245129](https://doi.org/10.1103/PhysRevB.104.245129)**I. INTRODUCTION**

Dirac semimetals (DSMs) that feature linear fourfold degenerate band crossing points, namely, Dirac points, near the Fermi level (E_f) have attracted broad interest in condensed physics and material science, because they manifest topologically protected Fermi arcs on surfaces and anomalous transport properties, including Shubnikov-de-Haas (SdH) oscillation, high carrier mobility, and chiral anomaly induced negative magnetoresistivity (MR) [1–3]. DSMs are categorized into type I, type II, and type III, according to the geometry of the bulk Dirac cone. Bulk Dirac points must be protected by crystalline symmetries and may split into a pair of Weyl points when either time-reversal or lattice inversion symmetry is broken. Currently investigated DSMs mainly focus on materials with both time-reversal and lattice inversion symmetries, such as Na₃Bi [4,5], Cd₃As₂ [6,7], and PtSe₂ class of transition metal dichalcogenides [8,9].

In noncentrosymmetric bulk materials, the absence of lattice inversion symmetry introduces an asymmetric potential gradient in the crystal, which generates an intrinsic Rashba-type antisymmetric SOC [10], removing the spin degeneracy of the bulk electronic bands. As such, a fourfold degenerate Dirac point in noncentrosymmetric materials is difficult to stabilize and rarely reported. In this paper, using first-principles calculations, we predict the coexistence of a topological insulator, type-II, and type-III Dirac fermions phases in the

bulk electronic band structure of noncentrosymmetric ternary equiatomic compounds LaPtSi and LaPtGe [11–16]. Electrical resistivity and magnetization measurements on LaPtSi and LaPtGe indicate that they exhibit phase transition to the superconducting state below temperature 3.8 [13] and 3.05 K [16], respectively. Temperature dependent specific heat under magnetic field analysis reveals that they could be categorized as Bardeen-Cooper-Schrieffer (BCS) superconductors with intermediate coupling [14,16]. Theoretical calculations predict that topologically protected Weyl nodal rings exist on the gliding mirror planes of these superconducting compounds around *X* points [17]. Noncentrosymmetric superconductors have been extensively studied for the ASOC results in a possible admixture of spin-singlet and spin-triplet pairing states [10,18].

Bulk Dirac points, coupled with *s*-wave bulk superconductivity, can support dispersive, helical Majorana fermions along the cores of superconducting vortices [19–21]. Majorana fermions, which can occur in certain solids, are particles identified with their own antiparticles and obey non-Abelian statistics [22], thus making them promising candidates for the use in fault-tolerant topological quantum computations [23–25]. Currently, the superconducting AB_2C class of full Heusler alloys [26–28], cubic superconductor YTi₃ [29], layered superconductor BaTi₂Bi₂O [30], iron-based superconductor LiFe_{1-x}Co_xAs [19–21], and Ir_{1-x}Pt_xTe₂ [31,32] are suggested as candidates for Dirac superconducting semimetal. However, there have been no reports on the experimental realization of helical Majorana modes in the above systems so far. Therefore, there is urgency in seeking promising material systems for the investigation of helical Majorana fermions.

*hithepeng@hit.edu.cn

†likanghit@hit.edu.cn

‡wzhao@hit.edu.cn

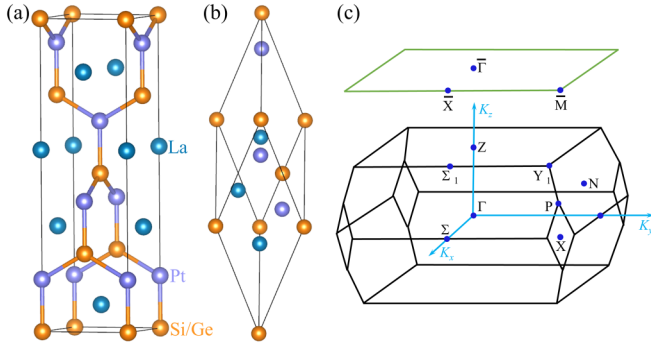


FIG. 1. Atomic structure of LaPtSi and LaPtGe shown as conventional (a) and primitive (b) cell forms. (c) Bulk BZ, (001) projected surface BZ, and high symmetry points.

II. METHODS

First-principles calculations were performed within the framework of the projector augmented wave (PAW) method [33,34] and selected the generalized gradient approximation (GGA) [35] with Perdew-Burke-Ernzerhof (PBE) type [36], as encoded in the Vienna *ab initio* simulation package (VASP) [37–39]. A kinetic energy cutoff of 500 eV and a Γ -centered k mesh of $12 \times 12 \times 12$ were utilized for all calculations. During self-consistent convergence and structural relaxation, the energy and force difference criteria were defined as 10^{-6} eV and 0.01 eV/Å. SOC was considered in a self-consistent manner. The WANNI90 package [40–42] was adopted to construct Wannier functions from the first-principles results. Topological property calculations were carried out by using WANNIERTOOLS code [43].

III. RESULTS AND DISCUSSION

LaPtSi and LaPtGe adopt the body-centered tetragonal noncentrosymmetric structure, which is a ternary variant of the α -ThSi₂ type structure [11–15], as shown in Fig. 1(a). Three nonequivalent atoms, including La, Pt, and Si (Ge) were placed in the $4a$ position of the $I4_1md$ space group (No. 109) with fractional coordinates: La $(0, 0, z_{La})$, Pt $(0, 0, z_{Pt})$, and Si (Ge) $(0, 0, 0)$. The structure is characterized by two sets of perpendicular Pt-Si (Pt-Ge) zigzag chains alternately stacked along the c axis. The optimized structural parameters, summarized in Table I, show reasonable agreement with the available experimental values [14,16]. All of the results presented in the following paragraphs are based on the optimized structural

TABLE I. Optimized lattice constants compared with available experimental values for LaPtSi and LaPtGe.

	LaPtSi	LaPtGe
a (Å)	4.2773	4.2965
c (Å)	14.6464	15.1578
	Experimental results	
a (Å)	4.2502 ^a	4.2655 ^b
c (Å)	14.5250 ^a	14.9654 ^b

^aReference [14].

^bReference [16].

TABLE II. Character table for the C_{4v} point group.

C_{4v}	E	C_{2z}	C_{4z}	M_x	M_{110}
Γ_1	1	1	1	1	1
Γ_2	1	1	-1	1	-1
Γ_3	1	1	-1	-1	1
Γ_4	1	1	1	-1	-1
Γ_5	2	-2	0	0	0
Γ_6	2	0	$-\sqrt{2}$	0	0
Γ_7	2	0	$\sqrt{2}$	0	0

parameters. The primitive unit cell containing two chemical formulas is shown in Fig. 1(b). The bulk Brillouin zone (BZ), projected (001) surface BZ, and high symmetry points are shown in Fig. 1(c).

The electronic band structure of LaPtSi obtained in the absence of SOC and presented in Fig. 2(a), unveils a three-dimensional (3D) metallic ground state with some bands featuring large energy dispersion across the E_f . Upon SOC inclusion, the band structure near the E_f was dramatically modified due to the strong SOC effects of La and Pt atoms and the absence of inversion center, as shown in Fig. 2(b). The degeneracy of some electronic bands happens to split at the high-symmetry points and between them, as can be observed in comparing Figs. 2(a) and 2(b). The overall band profiles consistent well with previous theoretical results [14]. In fact, the inversion symmetry of LaPtSi was broken solely by the particular stacking of the atoms along the out-of-plane direction, and the ASOC only affected the split energy levels along directions perpendicular to the c axis [14]. As such, the twofold degeneracy characteristics of the energy bands along the Γ -Z line still survive [see Fig. 2(b)].

The Dirac points are illustrated via the calculation of the irreducible representations (IRs) for related bands (Figs. 2 and 3). At the Γ point, the symmetry is characterized by the C_{4v} point group. In Table II we give the character table for C_{4v} . In the absence of SOC, the unoccupied valence band top at the Γ point belongs to nondegenerate IR Γ_1 . There is a band gap with a gap size of about 0.1 eV above the valence band top at the Γ point. The states lie above this gap at the Γ point can be labeled as doubly degenerate Γ_5 states. Under the double group representations in the presence of SOC, the Γ_5 states split into an upward shifted Γ_6 and a downward shifted Γ_7 states. The energy of the Γ_1 state remains consistent; only the IR changes to doubly degenerate Γ_6 . The Γ_6 states are energetically higher than the Γ_7 states, resulting in a band inversion,

TABLE III. The geometry types, topological charges (C), positions, and energies of Dirac points in LaPtSi and LaPtGe.

Compound	Type	C	$[0, 0, \pm k_z^D (\frac{2\pi}{c})]$	Energy (eV)
LaPtSi	I	0	0.5	0.36
	II	0	0.240	-0.343
	III	0	0.105	0.117
LaPtGe	I	0	0.5	0.43
	II	0	0.182	-0.242
	III	0	0.042	0.203

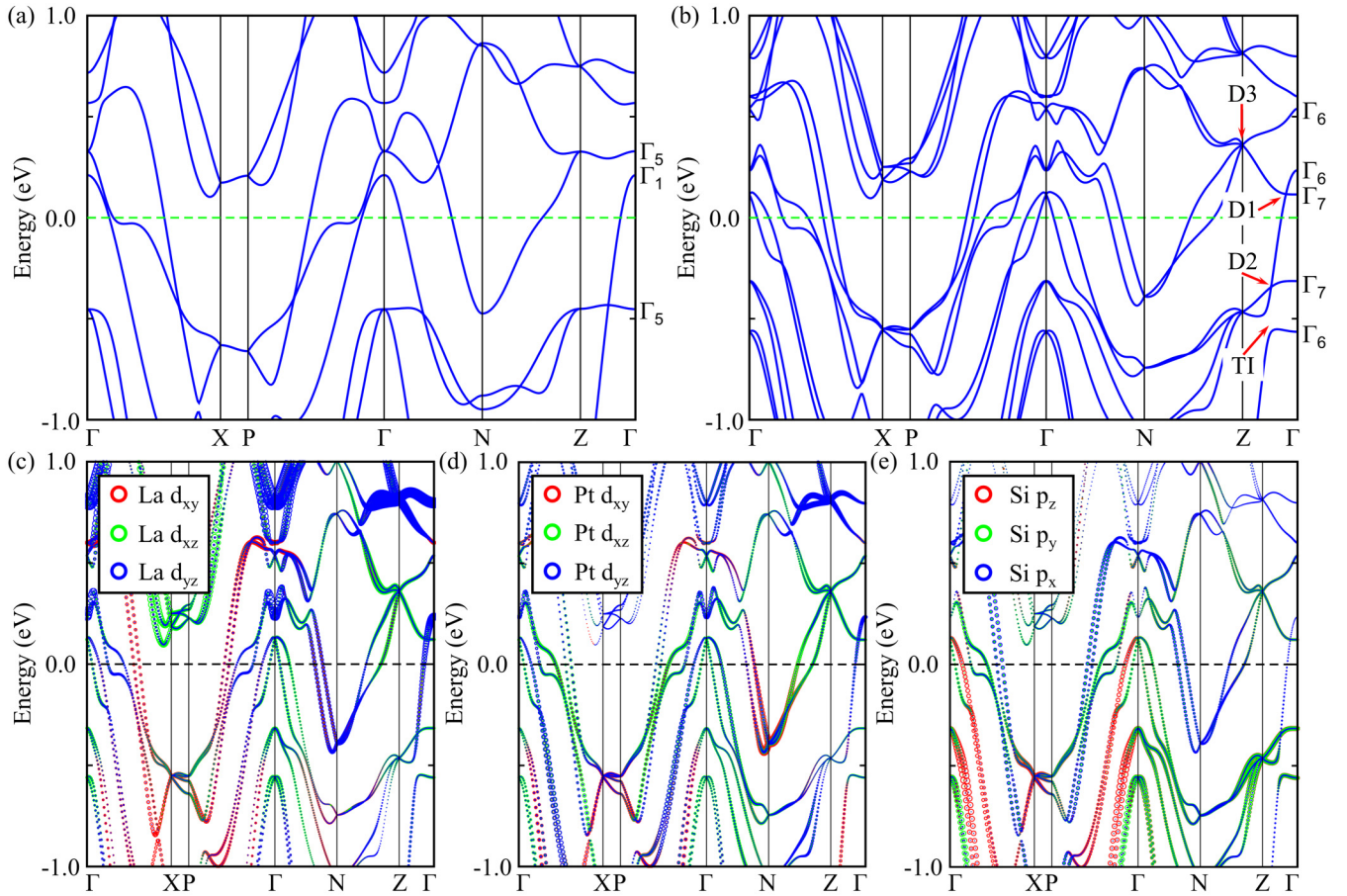


FIG. 2. Electronic band structure of LaPtSi obtained (a) in the absence and (b) in the presence of SOC. Γ_i indicates different IRs of selected bands. Band structures projected onto $5d$ orbitals of (c) La and (d) Pt atoms and $3p$ orbitals of (e) Si atoms.

which gives rise to nontrivial band topology of LaPtSi. The orbital projected band structures, plotted in Figs. 2(c)–2(e), show that the bands around the E_f are dominated by the La- $5d$, Pt- $5d$, and Si- $3p$ orbitals.

Along the Γ -Z direction, the little group is C_{4v} for any k point, the bands with Γ_6 and Γ_7 IRs at Γ point transform into Λ_6 and Λ_7 IRs, as shown in Figs. 3(a) and 3(b). Because the hybridization between the Λ_6 and Λ_7 bands under C_{4v} symmetry is strictly forbidden, one unavoidable band crossing appears at $(0, 0, k_z^D \approx \pm 0.105 \times \frac{2\pi}{c})$, which is denoted as D1 and clearly presented in Fig. 2(b). Since the energy bands forming D1 point along the Γ -Z line are doubly degenerate with linear dispersion and the calculated topological charge of D1 point is 0 (see in Table III), the band crossing is thus fourfold degenerate, or, namely, a Dirac point. The Dirac point D1 belongs to type III, because it is formed by the crossing of a flat band and a parabolic band [44,45], as shown in Figs. 3(a) and 3(d).

In the band structure without SOC, there is a triply degenerate band crossing point energy at 0.43 eV below the E_f along the Γ -Z direction, see Fig. 2(a). The triple point is formed by the touching of a nondegenerate band and a doubly degenerate band. The two relevant bands belong to Γ_1 and Γ_5 IRs at the Γ point. When SOC is included, there still presents a band crossing (denoted as D2) formed by two bands with different IRs (Λ_6 and Λ_7), see Fig. 3(b). Just like D1, D2 is a symmetry

protected fourfold degenerate Dirac point but belongs to type II, because the Dirac cone is tilted strongly along the Γ -Z [8], as shown in Figs. 3(b) and 3(e).

As shown in Figs. 2(c)–2(e), D1 and D2 are originated from the band inversion at the Γ point. The bands forming D1 are dominated by d_{xy} , d_{xz} , and d_{yz} orbitals. The bands forming D2 are dominated by p_y , p_z , and d_{yz} orbitals. D1 and D2 are thus accidental crossing points [46]. Intriguingly, the four bands crossing at the time-reversal invariant momenta (TRIM) point Z at 0.36 eV above the E_f , denoted as D3 in Fig. 2(b), is an essential crossing point. As shown in Figs. 3(c) and 3(i), the bands show linear dispersion around D3 along both the Γ -Z and Σ_1 -Z- Y_1 directions. The calculated topological charge of D3 point is 0 (see Table III). Thus, D3 is a Dirac point.

In addition to topological Dirac states, SOC also induces hybridization between two Λ_6 bands, leading to topological insulator (TI) states in the Γ -Z direction, see Fig. 2(b). We cut a curved Fermi level through the SOC induced TI gap, and calculated the \mathbb{Z}_2 invariant by using the Wilson loop method [47]. The calculated Wannier charge center (WCC) on two representative planes of the bulk BZ, shown in Fig. 4, evidence that $\mathbb{Z}_2 = 1$ for $k_z = 0$ plane, whereas $\mathbb{Z}_2 = 0$ for $k_z = \pi$ plane.

Different to the Dirac fermions in centrosymmetric compounds, where the twofold Dirac cone degeneracy is reserved at any k point in momentum space [4], the band degeneracy in

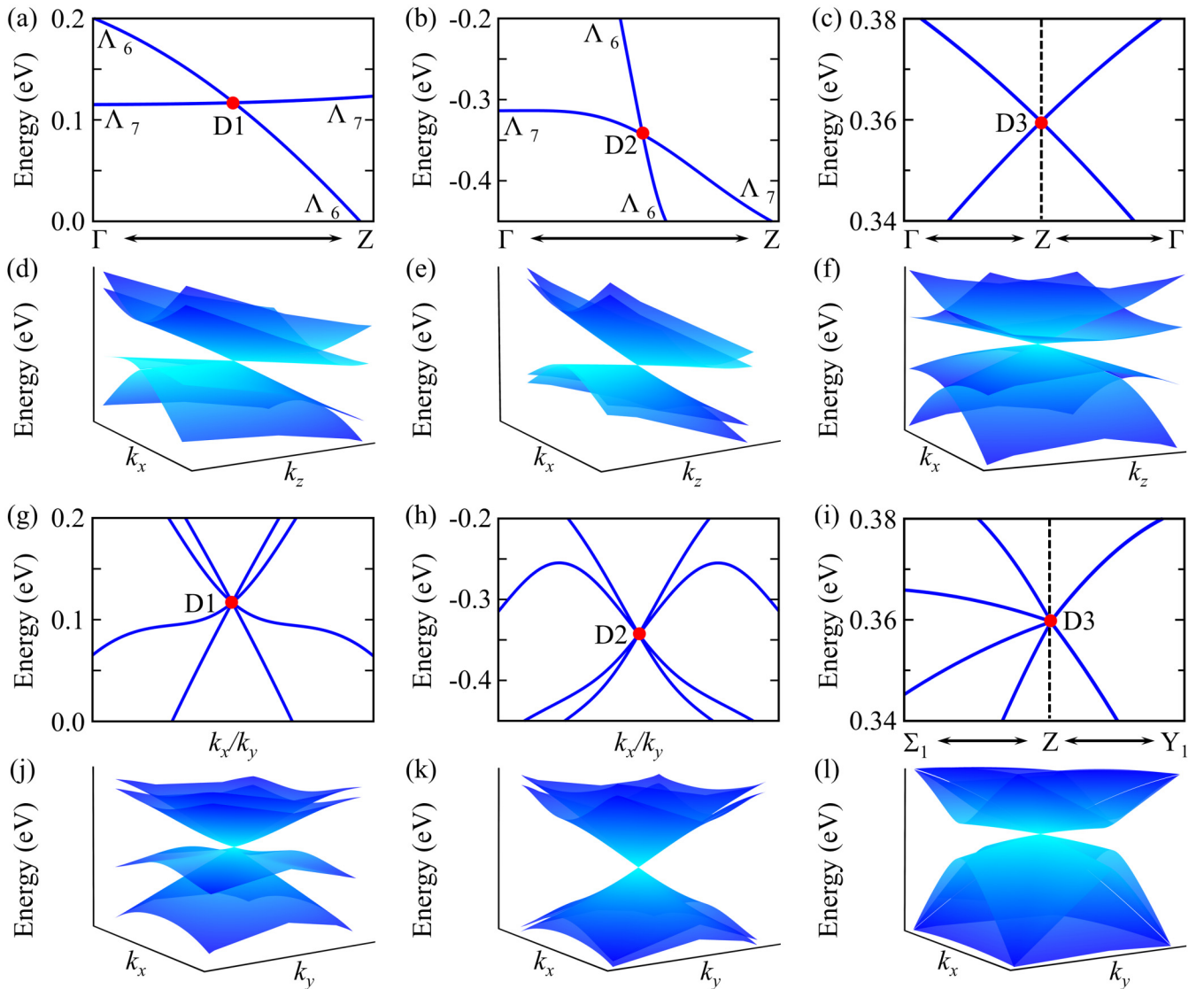


FIG. 3. The zoom-in band structures and the corresponding 3D dispersions around the band degeneracies labeled in Fig. 2(b): (a) and (b) The zoom-in band structures around D1 and D2 points along the Γ -Z direction. The IRs of related bands along the high symmetric k are indicated. (c) The enlarged band structures in the vicinity of D3 along the Γ -Z- Γ direction. (d)–(f) The 3D view of the three Dirac points in the k_x - k_z plane. (g)–(i) The in-plane band dispersions around D1, D2, and D3. (j)–(l) The 3D view of the three Dirac points in the k_x - k_y plane.

the k_x - k_y plane around the Dirac point in LaPtSi is completely removed due to the lack of inversion symmetry, as shown in Figs. 3(g)–3(l). The Dirac points here carry two cones with distinct slopes, resembles birefringent Dirac fermion, which have two “speeds of light,” and can be realized by using cold atoms in optical lattices [48–51]. Thus, birefringent Dirac fermions can also be achieved in noncentrosymmetric solid compounds.

The presence of topological nontrivial surface states on the surface is the hallmark of nontrivial bulk band topology. To further confirm the nontrivial topological nature of LaPtSi, we have carried out surface states calculations, the results are shown in Fig. 5. On the (001) surface, we observed multiple topological nontrivial surface states. Around the D3 point, the surface states (labeled as SS1) originating from D3 are clearly visible in Fig. 5(b). The Dirac cone type surface states (labeled as SS2) stemming from the projection of bulk type-III

Dirac points show large energy dispersion and lead the E_f crossing. Hence, they can make contributions to the transport properties. For the type-II Dirac states, due to the projection of D2, is hidden by the other bulk states, the sign of surface states (labeled as SS3) corresponding to D2 is partially observed. At about 0.5 eV below the E_f , due to the nontrivial \mathbb{Z}_2 TI gap, a Dirac cone surface state (labeled as SS4) emerges in the gapped bulk states. This surface Dirac cone exhibits a left-handed spin texture, as shown in Fig. 5(c).

Figure 6 depicts the bulk electronic band structure of LaPtGe in the absence and presence of SOC. The overall band profiles near the E_f of LaPtGe share resemble characteristics to those discussed for LaPtSi. It also hosts 3D Dirac points with substantial dispersions like LaPtSi. The positions and energies of Dirac points in these two materials are listed in Table III. Note that the type-II Dirac points in LaPtSi (LaPtGe) are 343 (242) meV lower than the E_f , which make

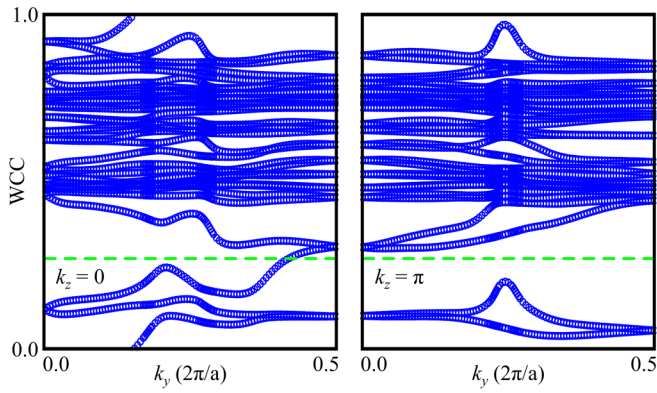


FIG. 4. Calculated evolution of Wannier charge centers for LaPtSi in the $k_z = 0$ and $k_z = \pi$ planes. The evolution lines pass through the reference line (green dashed line) at odd and even times in the $k_z = 0$ and π planes.

them easier to be observed by angle-resolved photoemission spectroscopy (ARPES). Compared to PtSe₂ classes of type-II DSMs [8], type-II Dirac points in our predicted compounds are much closer to the E_f , suggesting LaPtSi and LaPtGe are an improved platform for the study of type-II Dirac properties. Since the bulk type-III Dirac points are located above the E_f , it is not easy to directly detect them by ARPES. To observe the energy levels above the E_f , an *in situ* surface K atoms doping technique which dopes electrons into the surface layer can be used to shift the local chemical potential upward [5,52]. Since the type-III Dirac points in LaPtSi (LaPtGe) are only 117 (203) meV above the E_f , we hence expect that it could be probed by ARPES with the assistance of *in situ* surface K atoms doping.

Since the type-II and type-III Dirac points are located below and above the E_f , it is uncertain whether the bulk Dirac points become relevant to the superconductivity. Fortunately, the topological nontrivial surface states (SS2) feature a large dispersion in energy space and across the E_f , see Fig. 5(a).

To examine the stability of the crossing of the SS2 and the E_f , we have studied the effect of a surface potential on the SS2. Figures 5(d) and 5(e) present the calculated surface states with the on-site energy of the surface atoms changed to 110% and 120% of the pristine value, respectively. We find that the crossing of the SS2 and the E_f maintains at both considered values. Under natural superconducting proximity effects, the surface electrons will be induced into a superconducting phase, leading to equivalent $p + ip$ type superconductivity on the surface [53]. As such, the surface topological superconducting phase, which can host localized Majorana zero modes [54–56], is expected to exist in our predicted compounds. If the chemical potential can be tuned close to the bulk Dirac points by gate voltage or surface deposition, the bulk topological superconducting phase, which can support dispersive, helical Majorana modes [19–21], is also expected in currently studied noncentrosymmetric superconductors.

IV. SUMMARY

To summarize, we have presented the results of first-principles calculations on topological electronic structures for noncentrosymmetric BCS superconductors LaPtSi and LaPtGe. We predict the coexistence of three distinct types of topological nontrivial states, the topological insulator, type-II, and type-III Dirac fermions states, in their electronic band structure. We find that the type-II bulk Dirac points in LaPtSi (LaPtGe) are 343 (242) meV lower than the E_f , and much closer to it than the PtSe₂ class of type-II DSMs. The topological nontrivial surface states stemming from the projection of the type-III bulk Dirac points on the (001) surface show broad energy dispersion and lead to crossing of the E_f . As such, type-III Dirac points related exotic physics are detectable by transport experiments. Due to the coexistence of bulk Dirac fermions and bulk superconductivity, our predicted materials may be an exciting platform for investigating Dirac superconducting semimetal.

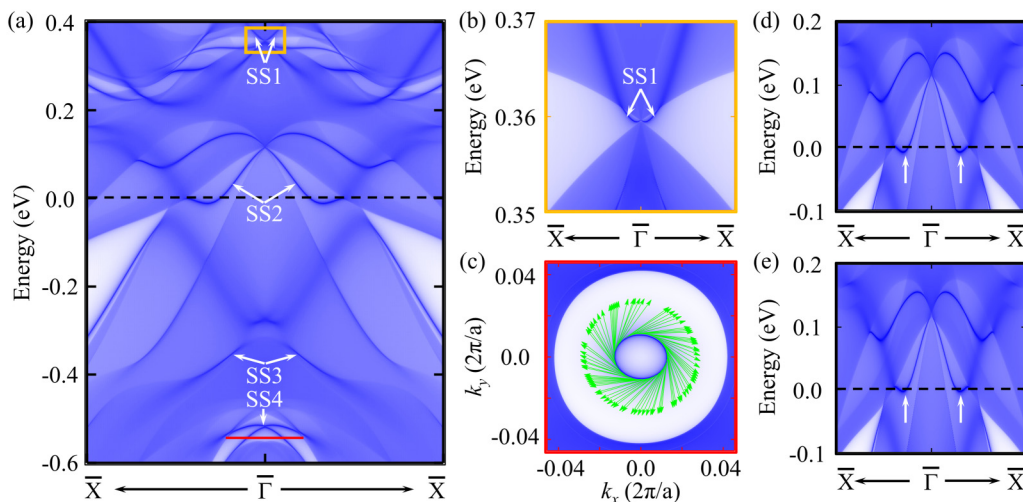


FIG. 5. (a) Calculated surface states of LaPtSi on the (001) surface. (b) Zoom-in view of the solid orange box region in (a). (c) Fermi surface of the topological state at -0.54 eV [marked in (a) with red line], the green arrows are the spin texture. Calculated surface states with the on-site energy of the surface atoms are changed to (d) 110% and (e) 120% of the pristine value. Arrows are guides to the eyes.

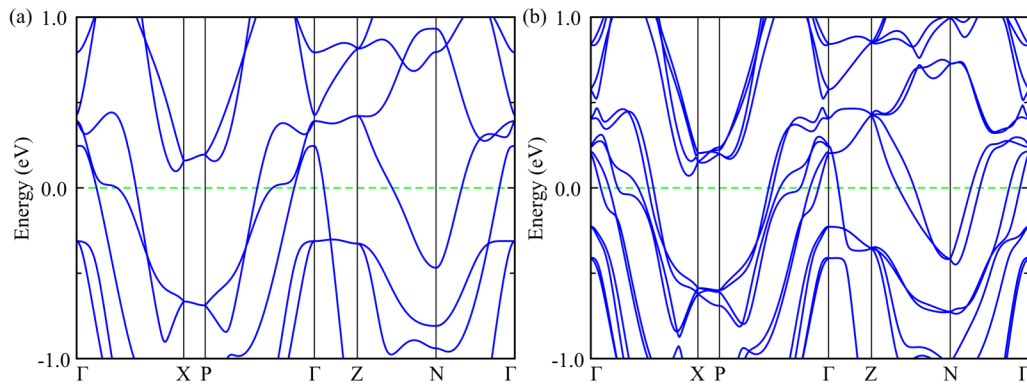


FIG. 6. Electronic band structure of LaPtGe (a) without and (b) with SOC considered.

ACKNOWLEDGMENTS

This work was supported by Shenzhen Science and Technology Program (Grants No. KQTD20170809110344233 and No. JCYJ20170811160129498), Bureau of Industry and

Information Technology of Shenzhen through the Graphene Manufacturing Innovation Center (Grant No. 201901161514), and Science and Technology Innovation Talents Program of Henan Province (Grant No. 174200510010).

- [1] H. M. Weng, X. Dai, and Z. Fang, *J. Phys.: Condens. Matter* **28**, 303001 (2016).
- [2] B. A. Bernevig, H. M. Weng, Z. Fang, and X. Dai, *J. Phys. Soc. Jpn.* **87**, 041001 (2018).
- [3] M. Hirayama, R. Okugawa, and S. Murakami, *J. Phys. Soc. Jpn.* **87**, 041002 (2018).
- [4] Z. Wang, Y. Sun, X.-Q. Chen, C. Franchini, G. Xu, H. Weng, X. Dai, and Z. Fang, *Phys. Rev. B* **85**, 195320 (2012).
- [5] Z. K. Liu, B. Zhou, Y. Zhang, Z. J. Wang, H. M. Weng, D. Prabhakaran, S.-K. Mo, Z. X. Shen, Z. Fang, X. Dai, Z. Hussain, and Y. L. Chen, *Science* **343**, 864 (2014).
- [6] Z. Wang, H. Weng, Q. Wu, X. Dai, and Z. Fang, *Phys. Rev. B* **88**, 125427 (2013).
- [7] Z. K. Liu, J. Jiang, B. Zhou, Z. J. Wang, Y. Zhang, H. M. Weng, D. Prabhakaran, S.-K. Mo, H. Peng, P. Dudin, T. Kim, M. Hoesch, Z. Fang, X. Dai, Z. X. Shen, D. L. Feng, Z. Hussain, and Y. L. Chen, *Nat. Mater.* **13**, 677 (2014).
- [8] H. Huang, S. Zhou, and W. Duan, *Phys. Rev. B* **94**, 121117(R) (2016).
- [9] K. Zhang, M. Yan, H. Zhang, H. Huang, M. Arita, Z. Sun, W. Duan, Y. Wu, and S. Zhou, *Phys. Rev. B* **96**, 125102 (2017).
- [10] L. P. Gor'kov and E. I. Rashba, *Phys. Rev. Lett.* **87**, 037004 (2001).
- [11] K. Klepp and E. Parthé, *Acta Crystallogr. Sect. B* **38**, 1105 (1982).
- [12] J. Evers, G. Oehlinger, A. Weiss, and C. Probst, *Solid State Commun.* **50**, 61 (1984).
- [13] S. Ramakrishnan, K. Ghosh, A. D. Chinchure, V. R. Marathe, and G. Chandra, *Phys. Rev. B* **52**, 6784 (1995).
- [14] F. Kneidinger, H. Michor, A. Sidorenko, E. Bauer, I. Zeiringer, P. Rogl, C. Blaas-Schenner, D. Reith, and R. Podloucky, *Phys. Rev. B* **88**, 104508 (2013).
- [15] S. Palazzese, J. F. Landaeta, D. Subero, E. Bauer, and I. Bonalde, *J. Phys.: Condens. Matter* **30**, 255603 (2018).
- [16] Sajilesh K. P., D. Singh, P. K. Biswas, A. D. Hillier, and R. P. Singh, *Phys. Rev. B* **98**, 214505 (2018).
- [17] P. Zhang, H. Yuan, and C. Cao, *Phys. Rev. B* **101**, 245145 (2020).
- [18] M. Smidman, M. B. Salamon, H. Q. Yuan, and D. F. Agterberg, *Rep. Prog. Phys.* **80**, 036501 (2017).
- [19] P. Zhang, Z. J. Wang, X. X. Wu, K. Yaji, Y. Ishida, Y. Kohama, G. Y. Dai, Y. Sun, C. Bareille, K. Kuroda, T. Kondo, K. Okazaki, K. Kindo, X. C. Wang, C. Q. Jin, J. P. Hu, R. Thomale, K. Sumida, S. L. Wu, K. Miyamoto *et al.* *Nat. Phys.* **15**, 41 (2019).
- [20] E. J. König and P. Coleman, *Phys. Rev. Lett.* **122**, 207001 (2019).
- [21] S. Qin, L. Hu, C. Le, J. Zeng, F.-C. Zhang, C. Fang, and J. Hu, *Phys. Rev. Lett.* **123**, 027003 (2019).
- [22] S. R. Elliott and M. Franz, *Rev. Mod. Phys.* **87**, 137 (2015).
- [23] A. Y. Kitaev, *Ann. Phys.* **303**, 2 (2003).
- [24] F. Wilczek, *Nat. Phys.* **5**, 614 (2009).
- [25] C. Nayak, S. H. Simon, A. Stern, M. Freedman, and S. Das Sarma, *Rev. Mod. Phys.* **80**, 1083 (2008).
- [26] P.-J. Guo, H.-C. Yang, K. Liu, and Z.-Y. Lu, *Phys. Rev. B* **95**, 155112 (2017).
- [27] P.-J. Guo, J.-F. Zhang, H.-C. Yang, Z.-X. Liu, K. Liu, Z.-Yi Lu, [arXiv:1811.06401](https://arxiv.org/abs/1811.06401).
- [28] C. Mondal, C. K. Barman, B. Pathak, and A. Alam, *Phys. Rev. B* **100**, 245151 (2019).
- [29] X.-H. Tu, P.-F. Liu, and B.-T. Wang, *Phys. Rev. Materials* **3**, 054202 (2019).
- [30] X. Shi, L. Chen, P. He, G. Wang, G. Zheng, X. Liu, and W. Zhao, *Phys. Rev. B* **99**, 155155 (2019).
- [31] F. C. Fei, X. Y. Bo, P. D. Wang, J. H. Ying, B. Chen, Q. Q. Liu, Y. Zhang, Z. Sun, F. M. Qu, Y. Zhang, J. Li, F. Q. Song, X. G. Wan, B. G. Wang, and G. H. Wang, *Adv. Mater.* **30**, 1801556 (2018).

- [32] B. B. Fu, C. J. Yi, Z. J. Wang, M. Yang, B. Q. Lv, X. Gao, M. Li, Y. B. Huang, C. Fang, H. M. Weng, Y. G. Shi, T. Qian, and H. Ding, [arXiv:1712.02500](#).
- [33] P. E. Blöchl, *Phys. Rev. B* **50**, 17953 (1994).
- [34] J. Lehtomäki, I. Makkonen, M. A. Caro, A. Harju, and O. Lopez-Acevedo, *J. Chem. Phys.* **141**, 234102 (2014).
- [35] J. P. Perdew and Y. Wang, *Phys. Rev. B* **45**, 13244 (1992).
- [36] J. P. Perdew, K. Burke, and M. Ernzerhof, *Phys. Rev. Lett.* **77**, 3865 (1996).
- [37] G. Kresse and J. Hafner, *Phys. Rev. B* **47**, 558 (1993).
- [38] G. Kresse and J. Furthmüller, *Comput. Mater. Sci.* **6**, 15 (1996).
- [39] G. Kresse and J. Furthmüller, *Phys. Rev. B* **54**, 11169 (1996).
- [40] A. A. Mostofi, J. R. Yates, Y.-S. Lee, I. Souza, D. Vanderbilt, and N. Marzari, *Comput. Phys. Commun.* **178**, 685 (2008).
- [41] N. Marzari and D. Vanderbilt, *Phys. Rev. B* **56**, 12847 (1997).
- [42] I. Souza, N. Marzari, and D. Vanderbilt, *Phys. Rev. B* **65**, 035109 (2001).
- [43] Q. S. Wu, S. N. Zhang, H. F. Song, M. Troyer, and A. A. Soluyanov, *Comput. Phys. Commun.* **224**, 405 (2018).
- [44] H. Huang, K.-H. Jin, and F. Liu, *Phys. Rev. B* **98**, 121110(R) (2018).
- [45] M. Milićević, G. Montambaux, T. Ozawa, O. Jamadi, B. Real, I. Sagnes, A. Lemaître, L. Le Gratiet, A. Harouri, J. Bloch, and A. Amo, *Phys. Rev. X* **9**, 031010 (2019).
- [46] B.-J. Yang and N. Nagaosa, *Nat. Commun.* **5**, 4898 (2014).
- [47] R. Yu, X. L. Qi, A. Bernevig, Z. Fang, and X. Dai, *Phys. Rev. B* **84**, 075119 (2011).
- [48] C. Chen, S.-S. Wang, L. Liu, Z.-M. Yu, X.-L. Sheng, Z. Chen, and S. A. Yang, *Phys. Rev. Material* **1**, 044201 (2017).
- [49] M. P. Kennett, N. Komeilizadeh, K. Kaveh, and P. M. Smith, *Phys. Rev. A* **83**, 053636 (2011).
- [50] B. Roy, P. M. Smith, and M. P. Kennett, *Phys. Rev. B* **85**, 235119 (2012).
- [51] N. Komeilizadeh and M. P. Kennett, *Phys. Rev. B* **90**, 045131 (2014).
- [52] P. Zhang, P. Richard, N. Xu, Y.-M. Xu, J. Ma, T. Qian, A. V. Fedorov, J. D. Denlinger, G. D. Gu, and H. Ding, *Appl. Phys. Lett.* **105**, 172601 (2014).
- [53] L. Fu and C. L. Kane, *Phys. Rev. Lett.* **100**, 096407 (2008).
- [54] P. Zhang, K. Yaji, T. Hashimoto, Y. Ota, T. Kondo, K. Okazaki, Z. J. Wang, J. S. Wen, G. D. Gu, H. Ding, and S. Shin, *Science* **360**, 182 (2018).
- [55] D. F. Wang, L. Y. Kong, P. Fan, H. Chen, S. Y. Zhu, W. Y. Liu, L. Cao, Y. J. Sun, S. X. Du, J. Schneeloch, R. D. Zhong, G. D. Gu, L. Fu, H. Ding, and H. J. Gao, *Science* **362**, 333 (2018).
- [56] Q. Liu, C. Chen, T. Zhang, R. Peng, Y. J. Yan, Chen-Hao-Ping, Wen, X. Lou, Y. L. Huang, J. P. Tian, X. L. Dong, G. W. Wang, W. C. Bao, Q. H. Wang, Z. P. Yin, Z.-X. Zhao, and D. L. Feng, *Phys. Rev. X* **8**, 041056 (2018).